CHIN. PHYS. LETT. Vol. 37, No. 9 (2020) 097402

Tunable Superconductivity in 2H-$NbSe_2$ via *In Situ* Li Intercalation

Kaiyao Zhou(周楷尧)[1,2], Jun Deng(邓俊)[1,2], Liwei Guo(郭丽伟)[1,2,3], and Jiangang Guo(郭建刚)[1,3*]

[1]*Beijing National Laboratory for Condensed Matter Physics, Institute of Physics, Chinese Academy of Sciences, Beijing 100190, China*

[2]*University of Chinese Academy of Sciences, Beijing 100049, China*

[3]*Songshan Lake Materials Laboratory, Dongguan 523808, China*

(Received 28 June 2020; accepted 20 July 2020; published online 1 September 2020)

Using the newly-developed solid ionic gating technique, we measure the electrical transport property of a thin-flake $NbSe_2$ superconductor (T_c = 6.67 K) under continuous Li intercalation and electron doping. It is found that the charge-density-wave transition is suppressed, while at the same time a carrier density, decreasing from 7×10^{14} cm^{-2} to 2×10^{14} cm^{-2} also occurs. This tunable capability in relation to carrier density is 70%, which is 5 times larger than that found using the liquid ionic gating method [Phys. Rev. Lett. 117 (2016) 106801]. Meanwhile, we find that the scattering type of conduction electrons transits to the *s*–*d* process, which may be caused by the change of the occupied states of 4*d*-electrons in Nb under the condition of Li intercalation. Simultaneously, we observe a certain decrement of electron-phonon coupling (EPC), based on the electron-phonon scattering model, in the high temperature range. Based on data gathered from *in situ* measurements, we construct a full phase diagram of carrier density, EPC and T_c in the intercalated $NbSe_2$ sample, and qualitatively explain the variation of T_c within the BCS framework. It is our opinion that the *in situ* solid ionic gating method provides a direct route to describing the relationship between carrier density and superconductivity, which is helpful in promoting a clearer understanding of electronic phase competition in transition metal dichalcogenides.

PACS: 74.25.Dw, 74.20.Fg, 71.15.Mb DOI: 10.1088/0256-307X/37/9/097402

Carrier density correlated to the electronic states at Fermi energy levels is an important factor affecting electronic phase transition.[1] Accurately calibrating the value of carrier density, the strengths of electron-electron interaction, and electron-phonon coupling (EPC) is crucial in terms of studying the origins of many emergent phenomena, such as magnetic phase transition,[2–5] the charge density wave (CDW),[6] and superconductivity (SC).[7–15] In Cu-based and Fe-based superconductors, complicated electronic phase diagrams have been constructed by tuning electron or hole density via introducing chemical substitution.[16–20] However, establishing an accurate relationship between carrier density, the strength of EPC, and the superconducting critical temperature (T_c) is still necessary in order to correctly understand multiple phase interactions and the microscopic mechanism. Recently, a field effect technique, using a high-κ dielectric of HfO_2 or BN as an insulating gate medium, has been developed to modulate the carrier density in thin-layer samples. This method can only induce carrier density variation in a maximum of about 10^{13} cm^{-2}, which may not cover the full range observed in SC.[21,22] More recently, with the aid of a solid ionic conductor, a new *in situ* gating technique has been shown to increase the carrier density of the sample by two orders of magnitude by means of the controllable intercalation of Li ions. Using this Li ion intercalation method, multiple superconducting phases in FeSe[23] and semiconductor-metal-superconductor transition in 1T-$SnSe_2$[24] have been found. In this work, by tracing the temperature-dependent transport property under gating, we clearly describe the relations between T_c, EPC and carrier density, with the aim of investigating the SC of 2H-$NbSe_2$.

It is well known that 2H-$NbSe_2$ is a type-Ⅱ superconductor with a T_c of about 7.3 K, higher than observed in most transition metal dichalcogenides. Moreover, a CDW phase transition, occurs at T_{CDW} = 33 K in bulk $NbSe_2$.[25] $NbSe_2$ possesses a hexagonal structure with a space group of $P6_3/mmc$, where a hexagonal plane of Nb atoms is sandwiched by two layers of Se atoms; each neutral $NbSe_2$ layer is connected by van der Waals force.[26] As the $NbSe_2$ is thinned to a monolayer, only one Nb-derived band crosses the E_F, leaving one hole-pocket both at Γ point and K point.[27] The CDW order in bulk and thin layer $NbSe_2$ has been extensively studied. Strengthened electron-phonon coupling,[28,29] enhanced Fermi-surface nesting,[30,31] and saddle-point singularities[32] have also been reported recently.

Supported by the MoST-Strategic International Cooperation in Science, Technology and Innovation Key Program (Grant No. 2018YFE0202601), the National Key Research and Development Program of China (Grant Nos. 2017YFA0304700 and 2016YFA0300600), the National Natural Science Foundation of China (Grant Nos. 51922105 and 51772322), and the Chinese Academy of Sciences (Grant No. QYZDJ-SSW-SLH013).

*Corresponding author. Email: jgguo@iphy.ac.cn

© 2020 Chinese Physical Society and IOP Publishing Ltd

Here, we systemically tune the carrier density, EPC constant and SC in a thin layer $NbSe_2$ sample, using the solid-ionic-conductor gating technique, where intercalation of Li ions into $NbSe_2$ layers is controlled by an external electric field. Following a detailed analysis of the transport data, we find that the T_c continuously decreases below 1.5 K as the carrier density decreases and EPC is weakened. The decreased amount of carrier density is over 70%, which significantly exceeds the tunable capability of sole electrostatic doping in the ionic liquid technique. A superconducting phase diagram is constructed, based on our measurements, where the decrement of T_c is explained by decreased carrier density and weakened EPC within the BCS framework.

Experimental Details. Bulk $NbSe_2$ single crystals were grown by a conventional chemical vapor deposition method, with iodine as a transport agent. The stoichiometric mixture of high-purity Nb powder (Alfa Aesar, 99.99%) and Se powder (Alfa Aesar, 99.999%) was sealed in an evacuated quartz tube (15 cm long), before being placed in a two-temperature zone tube furnace. The temperatures were set to 900 K and 800 K, respectively, and the growth process took place over two weeks. The typical single crystals were plate-like, with a size of 0.01 mm × 0.5 mm × 2 cm. The crystal structure was verified using a Panalytical X'pert PRO diffractometer (Cu $K\alpha$ radiation) with a graphite monochromator in the 2θ range from 5° to 130°.

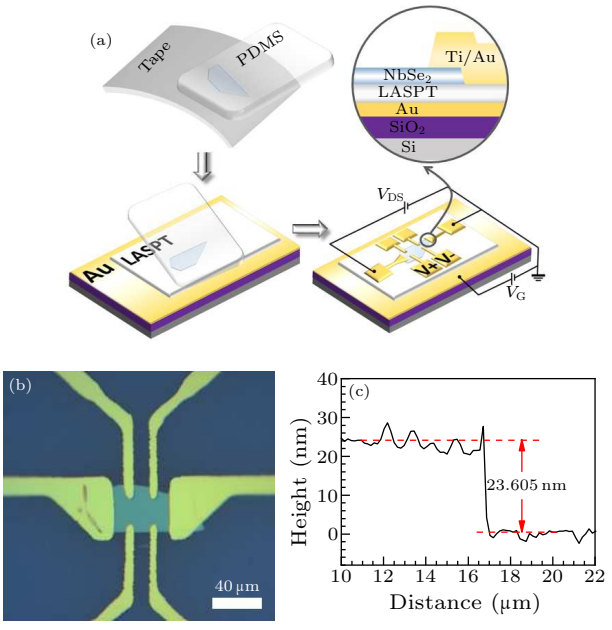

Fig. 1. Schematic fabrication process for a thin-flake $NbSe_2$ device, and its analysis via optical microscopy and AFM. (a) Schematic process for the device. (b) Optical image of the device. Scale bar 40 μm. (c) Sample thickness measured by AFM.

In a typical fabrication process, a 50 nm Au layer was first deposited on a SiO_2 (270 nm)/Si substrate by electronic beam evaporation. Next, $Li_2Al_2SiP_2TiO_{13}$ (LASPT) (KEJING Co. Ltd) was pasted onto the Au deposited substrate using silver conductive epoxy. A schematic of this process is shown in Fig. 1(a). A semi-transparent thin flake (size over 50 × 30 μm^2) of $NbSe_2$ was prepared by mechanical exfoliation from $NbSe_2$ single crystals, then transferred onto LASPT using polydimethylsiloxane (PDMS). A Hall bar with Ti(10 nm)/Au(100 nm) electrodes was then patterned onto the thin-flake, using e-beam lithography, as shown in Fig. 1(b). The sample surface was observed via optical spectroscopy (Olympus BX51). Its thickness of 20–80 nm was determined by atomic force microscopy (AFM) (Bruker AFM Multimode 8) [see Fig. 1(c)]. The sample's transport property was measured inside a closed-cycle cryostat (C-mag 9 T), equipped with a Keithley 2182 A and a 2400 source meter. Back-gated voltage $V_G = 5.5$ V was applied to the LASPT, since the electrochemical window of LASPT is below 6 V.

First principles calculations were performed using the Vienna *ab initio* simulation package (VASP).[33,34] We adopted the generalized gradient approximation (GGA) in the form of the Perdew–Burke–Ernzerhof (PBE) functional[35] for the exchange-correlation potentials. The projector augmented-wave (PAW) pseudopotential[36] was employed, with a plane-wave energy cutoff of 500 eV. The $Li_{0.33}NbSe_2$ was simulated by a 3 × 3 × 1 supercell of $LiNbSe_2$ with random Li vacancies. Monkhorst–Pack[37] k-meshes of 17 × 17 × 4 and 6 × 6 × 4 were used for sampling the first Brillouin zone in the self-consistent calculation, and 34 × 34 × 8 and 11 × 11 × 8 were used for the density of states for $NbSe_2$ and $Li_{0.33}NbSe_2$, respectively. Atomic positions and lattice parameters were relaxed until all the forces on the ions were less than 10^{-2} eV/Å.

Results and Discussion. Figure 2(a) shows an optical image of bulk single crystal $NbSe_2$ with a shiny surface. The lattice constant along the c-axis, 12.548 Å, was determined by the (002) peak position of the x-ray diffraction pattern depicted in Fig. 2(b). As shown in Fig. 2(c), the molar ratio of Nb and Se is 38.15 : 61.85, which is close to nominal composition, regardless of the intrinsic errors associated with energy dispersive spectroscopy. Layered morphology and hexagonal symmetry can be observed in the image from the scanning electron microscope (SEM). The temperature dependence of electrical resistivity in bulk $NbSe_2$ was measured through the standard four-electrode method. Figure 2(d) shows a T_c^{onset} of 7.27 K, and the residual resistance ratio (RRR) $R_s(300\,K)/R_s(8\,K)$ is about 12.85.

As is well known, mechanical exfoliation is a convenient method for obtaining high quality and thin-flake samples from a single crystal.[26] The PDMS dry-transfer method does not require any wet chemistry, thereby maintaining the purity of the sample.[38] We

fabricated a hall bar on thin-flake $NbSe_2$ via a process of mechanical exfoliation and the PDMS dry-transfer method. In this work, the thickness of the thin-flake $NbSe_2$ is around 20–80 nm. The transport properties of the thin-flake sample were measured as shown in Fig. 2(e). It is observed that a sharp superconducting transition appears in the sheet electrical resistance (R_s) curve, measured from 300 K to 1.5 K. The onset of superconducting critical temperature (T_c^{onset}) is 6.67 K and T_c^{zero} is 6.65 K. The RRR of the thin-flake $NbSe_2$ is 16.95, even higher than that for bulk $NbSe_2$, demonstrating the high quality of the sample. To estimate the upper critical fields [$H_{c2}(T)$] of the thin-flake $NbSe_2$, we systematically measured the temperature-dependent $R_s(T)$ in applied magnetic fields. Figure 2(f) shows the corresponding results for H, perpendicular to the (001) plane. The $H_{c2}(T)$ is determined by using a 10% drop in normal state resistance (R_n). A satisfactory fitting of the curve of $H_{c2}(T)$ by the Ginzburg–Landau model, $H_{c2}(T) = (\varphi_0/2\pi\xi^2)[1-(T/T_c)^b]$, is obtained, where φ_0 is the flux quantum 2.067×10^{-15} Wb and ξ the superconducting coherence length. The $\mu_0 H_{c2}(0)$ is derived to be 2.39 T. According to the relationship, $\mu_0 H_{c2}(0) = \varphi_0/2\pi\xi^2$, the value of ξ is derived to be 11.73 nm.

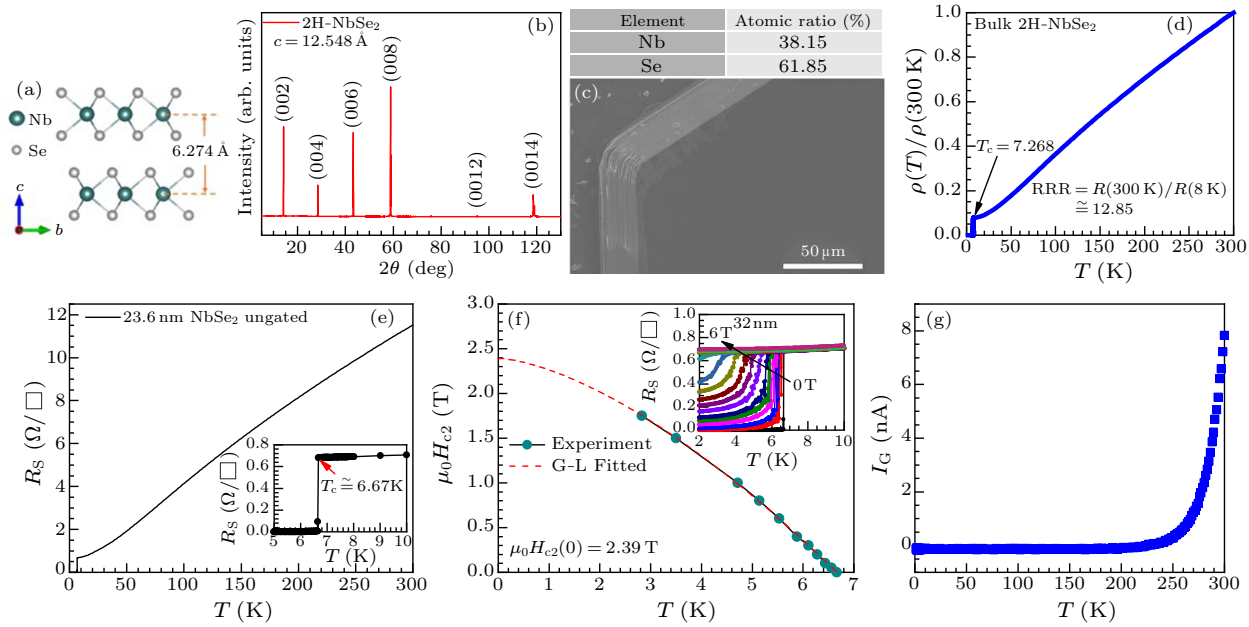

Fig. 2. (a) Crystal structure of 2H-$NbSe_2$. (b) X-ray diffraction pattern of $NbSe_2$ single crystal. Inset: optical image of as-grown $NbSe_2$ on a 1 mm × 1 mm grid. (c) SEM image of $NbSe_2$. Scale bar is 50 μm. (d) Normalized temperature dependence of electrical resistivity of bulk $NbSe_2$. (e) Temperature dependence of R_s of the thin $NbSe_2$ sample. The enlarged section of R_s at low temperature is shown as an inset. (f) Upper critical field ($\mu_0 H_{c2}$) as a function of temperature. Inset: temperature dependence of R_s subject to an external magnetic field. (g) Temperature dependence of I_G with a gate voltage of 5.5 V.

In order to select a suitable gating temperature, we measure the temperature dependence of the leakage current I_G [see Fig. 2(g)]. We find that I_G is almost independent of the temperature at $T < 170$ K, and there is only a tiny negative noise current, given that the Li ions are still frozen in LASPT. In the temperature range from 170–250 K, I_G slowly increases, and for $T > 250$ K, the I_G steeply increases. Based on the temperature dependence of I_G, we select a gating temperature between 170–300 K. Based on the dependence of I_G on temperature and gating voltage, we set the gating voltage to 5.5 V for the experiment below.

Figure 3(a) illustrates the temperature dependence of R_s, measured in a temperature range below 200 K, after 5.5 V gating for one hour at the selected gating temperature range. As the gating temperature increases, the Li ions in the LASPT are more active and migrating more readily into the space between the $NbSe_2$ layers. As a result, T_c gradually decreases below 1.5 K, which is beyond our measurement limit, and SC is suppressed. Moreover, the slope of the resistance curve levels off, suggesting the weakening of electron-phonon coupling strength. In addition, we do not observe a clear kink in the resistance curve at the proposed $T_{CDW} = 33$ K, which is consistent with the electrical resistivity features of $NbSe_2$ reported in Refs. [39,40]. To examine the kink feature of resistivity in detail, we take the first-order derivative of the $R_s(T)$ curves, as shown in Fig. 3(b); a kink can be faintly observed in pristine and slightly intercalated samples at around 25 K, and close to 33 K, the reported T_{CDW} for bulk $NbSe_2$, suggesting that this phenomenon is a signature of CDW transition. Having applied electric-field gating above 280 K, the kink in the first-order derivative (dR_s/dT) disappears, implying the suppression of CDW transition.

After each gating, we measured the magnetic field dependence of Hall resistance R_{xy} so as to deduce the sheet's carriers density n_{2D}. The data are plotted in Fig. 3(c). A single-band model was used to fit the R_{xy}, from which we can calculate hall coefficient R_H by $R_H = R_{xy}/B$. The n_{2D} was derived from the equation $n_{2D} = 1/(eR_H)$, where e denotes the electron charge. The n_{2D} as a function of temperature is plotted in Fig. 3(d). For the pristine flake $NbSe_2$, the character of the major carrier changes from hole to electron below 30 K; this Lifshitz transition may be a signature of the CDW transition.[41] Comparing the difference in n_{2D} at 50 K, we discover that the tunable ability of carrier density (Δn_{2D}) is about $2.59 \times 10^{15}\,\mathrm{cm}^{-2}$, which is nearly 5 times the value $6 \times 10^{14}\,\mathrm{cm}^{-2}$ obtained via ionic liquid gating.[42] Therefore, we have established that our gating technique can induce a much greater variation in carrier density, which also results in a wide variation in T_c. Both of these factors provide further information relating to the study of SCs.

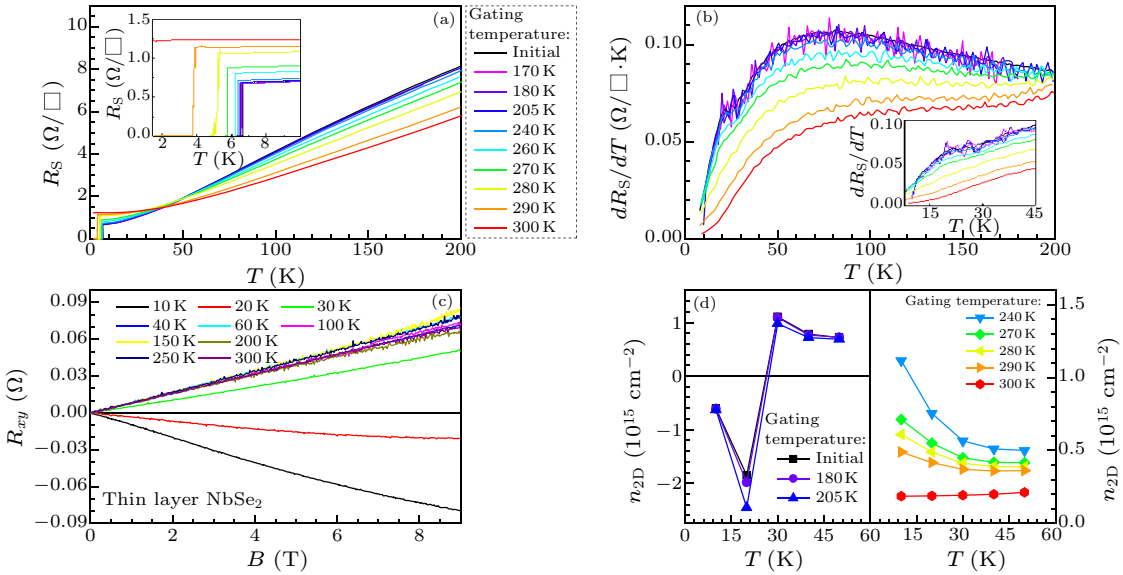

Fig. 3. Transport properties of thin-flake $NbSe_2$ subsequent to gating in the selected gating temperature range from 170 K to 300 K. (a) Temperature-dependent R_s. Inset: an expanded view of the low temperature range. (b) The first derivative of R_s on $T_c^{onset} < T < 200$ K. Lower right inset gives an enlarged view of CDW transitions at low temperature. (c) Field dependence of R_{xy}. (d) Temperature dependence of the n_{2D}.

At low temperatures, the R_s can be fitted by the following power law function:

$$R_s = R_0 + AT^{\alpha},$$

where R_0 denotes the residual square sheet resistance that is independent of temperature, A is a constant, and α represents the exponent index, which is critically dependent on the type of interaction. The fitting was performed from the T_c to 30 K [see Fig. 4(a)]. For a conventional metal, described by the Fermi liquid theory, the α is 2. By increasing the amount of Li ions, the α increases to 3, indicating that the nature of the interaction turns from itinerant electron-electron interaction to the s–d electron scattering variety. Similar interactions between s and d bands have been observed for NbC and TaC.[43] Here, the Li intercalation lowers the chemical valence of Nb^{4+}, and the increase of $4d$ electrons may be responsible for inducing the observed change in the scattering process. Meanwhile, we find that the residual resistance R_0 has also increased monotonously, implying that many more scattering sites are created with increased Li-intercalation. The T_c-dependent α is plotted on the upper panel of Fig. 4(b), where the α is shown to have rapidly increased as the T_c gradually decreases.

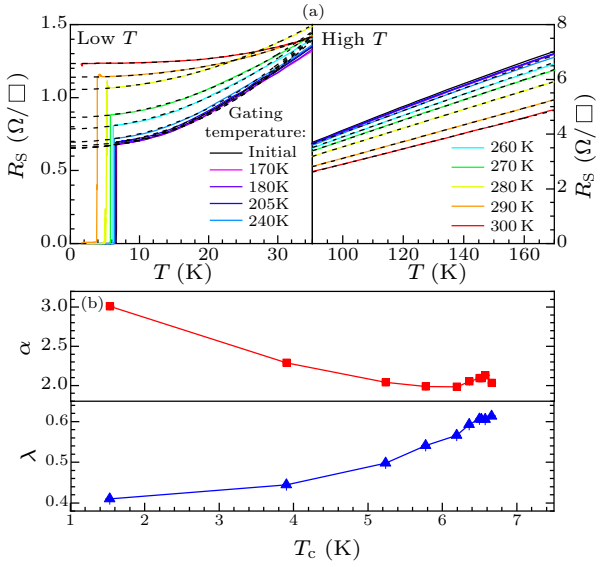

Fig. 4. Transport properties of thin $NbSe_2$. (a) Temperature-dependent R_s and the fitted results based on the formula $R_s = R_0 + AT^{\alpha}$ (red curve), and the electron-phonon scattering model in the high-temperature limit (green curve). (b) Variation of α and λ versus T_c.

Furthermore, we fit the curve of high temperature range based on the electron-phonon scattering model in the high-temperature limit, so as to estimate the strength of EPC in intercalated thin-flake $NbSe_2$. In quasi-2D systems, the formula is given as follows:[39]

$$R_s(T) \approx R_0 + \lambda \frac{2\pi k_B m}{\hbar e^2 n_{2D}} T = R_0 + \lambda \frac{2\pi\hbar n_0 k_B}{\varepsilon_0 n_{2D} (\hbar\omega_{p0})^2} T,$$

where λ, $\hbar$, and k_B correspond to an EPC constant, Planck's constant and the Boltzmann constant, respectively, and n_0 denotes bulk carrier density. The sheet carrier density is $n_{2D} = n_0 \times d$, with d being the sample thickness. Here, ω_p denotes the plasma frequency, $\omega_{p0} = \sqrt{n_0 e^2/\varepsilon_0 m}$ with ε_0 is the vacuum permittivity, and $\hbar\omega_{p0} = 2.74\,\text{eV}$ for bulk $NbSe_2$.[44] The fitting data and obtained λ are plotted in the right panel of Fig. 4(a) and the lower panel of Fig. 4(b), respectively. For pristine thin-flake $NbSe_2$, the λ is 0.61, implying that $NbSe_2$ is an intermediately coupled superconductor. We find that λ decreases as the injection amount of Li ions increases, and that the smallest λ is 0.41.

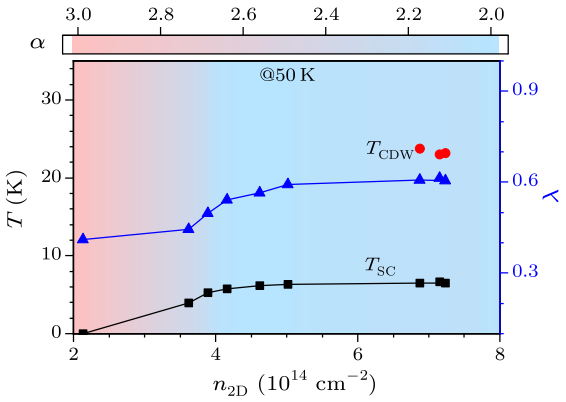

Fig. 5. Summarized T_{CDW}, λ and T_c in gated $NbSe_2$. Red solid circles correspond to the T_{CDW}, defined as the sign change of R_H. Black solid squares represent the T_c. The blue solid triangle represents the scale of EPC constant. The color shade shows the transition of α, implying the change of the electron interaction.

Figure 5 summarizes the carrier density relationships, T_c and λ, in the Li-ion intercalated thin-flake $NbSe_2$. Note that T_c remains nearly unchanged until n_{2D}, less than $5 \times 10^{14}\,\text{cm}^{-2}$, then gradually decreases. For the sake of accuracy, we only plot the T_{CDW} determined from the sign change of R_H, as shown in Fig. 3(b). The T_{CDW} seems to show a slight increase when T_c decreases. The color contrast bar at the top of Fig. 5 represents the α values calculated from the fitting of $R_s = R_0 + AT^\alpha$. As the T_c decreases, the α increases from 2 to 3, indicating that the s–d electron scattering becomes dominant. It is understood that the intercalation of Li ions into FeSe[23] and $SnSe_2$,[24] driven by an electric field, favors SC in FeSe and $SnSe_2$, where the increased electron density plays a decisive role. The increase of electron density also induces a great change in the carrier density of $NbSe_2$, as analyzed via Hall measurement, such that the hole carrier value n_{2D} reduces by $2.59 \times 10^{15}\,\text{cm}^{-2}$. However, in Li-intercalated $NbSe_2$, the T_c is only monotonously suppressed with an increase in the gating temperature, which is consistent with the trend in the Li_xNbSe_2 powder sample prepared by the solid-state reaction method.[45] As x is about 0.3, the SC is suppressed by slightly increasing the lattice constants. However, this is different from the feature of Rb_xNbSe_2,[46] where intercalation of large size Rb^+ cations changes both crystal and electronic structures, and even suppresses the SC transition below 1% doping.

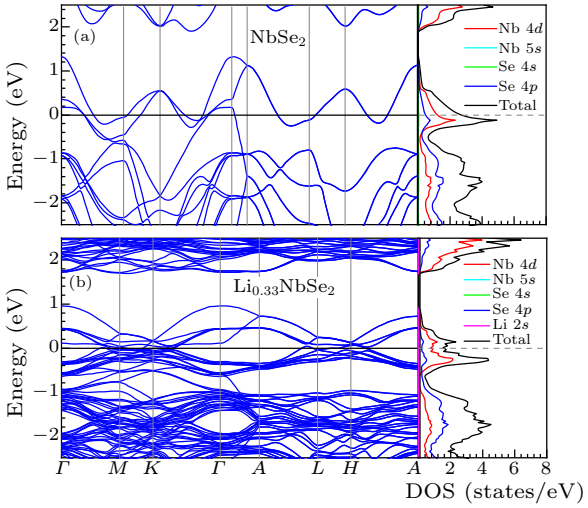

Fig. 6. Energy band structures (left) and projected density of states (right) normalized as per formula for (a) $NbSe_2$ and (b) $Li_{0.33}NbSe_2$.

Our *in situ* Li-intercalation technique barely alters the structural symmetry and Nb–Se bond length. For a qualitative understanding of the evolution of the electronic structure, we calculate the energy band structures and projected density of state (PDOS) for $NbSe_2$ and hypothetical $Li_{0.33}NbSe_2$, as shown in Fig. 6. As we know, in a metal, the variation in carrier density due to Li intercalation should be determined by the specific location of Fermi energy E_F. Assuming that the E_F lies at a valley (peak) of the density of states, the intercalation of Li^+ should push the E_F away from the valley (peak) thereby increasing (decreasing) the carrier density under the rigid model. In the $NbSe_2$ sample, theoretical calculations show that the E_F is almost at the peak of the density of states. Intercalating Li^+ drives the E_F away from the peak, lowering the value of 2.65 states/eV per formula to 1.50 states/eV per formula. Our experimental data also confirms that the carrier density is decreased from $7\times10^{14}\,\text{cm}^{-2}$ to $2\times10^{14}\,\text{cm}^{-2}$, which supports the trend indicated by the theoretical calculations. The states around E_F are primarily composed of the Nb-4d and Se-4p orbital states for both $NbSe_2$ and $Li_{0.33}NbSe_2$. In the $Li_{0.33}NbSe_2$, where there is

still metallic conductivity, even the Fermi surface lifts a little bit. Further lifting the E_F to the gap between 1.2 eV and 2.0 eV would lead to semiconducting behavior. According to the BCS theory, the SC gap $\Delta = 2\hbar\omega_L \exp[-1/N(E_F)\lambda]$, occurs where $\hbar\omega_L$ is the average phonon energy, and $N(E_F)$ is the density of state at the E_F. In the present work, the intercalated Li directly reduces the values of $N(E_F)$ and λ; as a result, the T_c is decreased.

In summary, we have observed that the T_c in $NbSe_2$ is gradually suppressed due to Li ionic intercalation and being subject to electric gating. According to the BCS theory, the suppression of T_c of the thin-flake $NbSe_2$ is explained by the mutual effect of reduced density of state at the E_F, and the weakened interaction of electron-phonon coupling. This *in situ* solid gating method allows the carrier density to be tuned over a wide range, and may enable us to accurately identify multiple important physical parameters critically affecting the SC, providing conclusive evidence in terms of understanding the superconducting evolution of $NbSe_2$.

References

[1] Zhang S *et al.* 2018 *Chin. Phys. Lett.* **35** 097401
[2] Deng Y J *et al.* 2018 *Nature* **563** 94
[3] Shimamura K *et al.* 2012 *Appl. Phys. Lett.* **100** 122402
[4] Matsukura F, Tokura Y and Ohno H 2015 *Nat. Nanotechnol.* **10** 209
[5] Klein D R *et al.* 2018 *Science* **360** 1218
[6] Li L J *et al.* 2016 *Nature* **529** 185
[7] Qin F *et al.* 2018 *Nano Lett.* **18** 6789
[8] Nakagawa Y *et al.* 2018 *Phys. Rev. B* **98** 064512
[9] Yuan H T *et al.* 2013 *Nat. Phys.* **9** 563
[10] Shimizu S *et al.* 2013 *Phys. Rev. Lett.* **111** 216803
[11] Zhang Y J, Ye J T, Matsuhashi Y and Iwasa Y 2012 *Nano Lett.* **12** 1136
[12] Nakano M *et al.* 2012 *Nature* **487** 459
[13] Cui Y *et al.* 2019 *Chin. Phys. Lett.* **36** 077401
[14] Mao Y Y *et al.* 2018 *Chin. Phys. Lett.* **35** 057402
[15] Zhang X *et al.* 2019 *Chin. Phys. Lett.* **36** 057402
[16] Croft T P *et al.* 2014 *Phys. Rev. B* **89** 224513
[17] Keimer B *et al.* 2015 *Nature* **518** 179
[18] Ying T P *et al.* 2013 *J. Am. Chem. Soc.* **135** 2951
[19] Ren Z A *et al.* 2008 *Chin. Phys. Lett.* **25** 2215
[20] Sun R J *et al.* 2018 *Phys. Rev. B* **98** 214508
[21] Fatemi V *et al.* 2018 *Science* **362** 926
[22] Chen Z Y *et al.* 2018 *Nat. Commun.* **9** 4008
[23] Ying T P *et al.* 2018 *Phys. Rev. Lett.* **121** 207003
[24] Song Y P *et al.* 2019 *Phys. Rev. Mater.* **3** 054804
[25] Ugeda M M *et al.* 2016 *Nat. Phys.* **12** 92
[26] Wang H, Huang X, Lin J *et al.* 2017 *Nat. Commun.* **8** 394
[27] Zehetmayer M and Weber H W 2010 *Phys. Rev. B* **82** 014524
[28] Weber F *et al.* 2011 *Phys. Rev. Lett.* **107** 107403
[29] Varma C M and Simons A L 1983 *Phys. Rev. Lett.* **51** 138
[30] Straub Th *et al.* 1999 *Phys. Rev. Lett.* **82** 4504
[31] Borisenko S V *et al.* 2009 *Phys. Rev. Lett.* **102** 166402
[32] Kiss T *et al.* 2007 *Nat. Phys.* **3** 720
[33] Kresse G and Furthmüller J 1996 *Comput. Mater. Sci.* **6** 15
[34] Kresse G and Furthmüller J 1996 *Phys. Rev. B* **54** 11169
[35] Perdew J P, Burke K and Ernzerhof M 1997 *Phys. Rev. Lett.* **78** 1396
[36] Kresse G and Joubert D 1999 *Phys. Rev. B* **59** 1758
[37] Monkhorst H J and Pack J D 1976 *Phys. Rev. B* **13** 5188
[38] Frisenda R *et al.* 2018 *Chem. Soc. Rev.* **47** 53
[39] Arguello C J *et al.* 2014 *Phys. Rev. B* **89** 235115
[40] Edwards J and Frindt R F 1971 *J. Phys. Chem. Solids* **32** 2217
[41] Zhang S S, Ye J W and Liu W M 2016 *Phys. Rev. B* **94** 115121
[42] Xi X X *et al.* 2016 *Phys. Rev. Lett.* **117** 106801
[43] Allison C Y, Finch C B, Foegelle M D and Modine F A 1988 *Solid State Commun.* **68** 387
[44] Dordevic S V, Basov D N, Dynes R C and Bucher E 2001 *Phys. Rev. B* **64** 161103
[45] McEwen C S, St D J, Edwards P P and Sienko M J 1985 *Inorg. Chem.* **24** 1656
[46] Fan X *et al.* 2019 *Inorg. Chem.* **58** 7564